Experimental Determination of the Impulse Coupling Coefficient - Standardization Issues

S. Scharring[a], J. E. Sinko[b], A. Sasoh[c], H.-A. Eckel[a] and H.-P. Röser[d]
[a]Institute of Technical Physics, German Aerospace Center, Stuttgart, Germany
[b]Micro-Nano Global Center of Excellence, Nagoya University, Japan
[c]Department of Aerospace Engineering, Nagoya University, Japan
[d]Institute of Space Systems, University of Stuttgart, Germany

Abstract
In research on beamed energy propulsion, the momentum coupling coefficient c_m is a central figure of merit to characterize a propulsion system. The determination of c_m is based on the measurement of imparted impulse and laser pulse energy. Nevertheless, the knowledge of laser pulse length, laser spot area and ablated mass is of great importance for the comparability of experimental results in laser ablative propulsion. The use of a great variety of measurement techniques for these parameters throughout the scientific community implies the risk of misunderstandings and might impede the comparability of results. In this paper, we present critical issues concerning the measurement of the aforementioned key parameters with respect to possible standardization issues. As an example, a simple laser propulsion experiment will be presented and compared with an experimental model from a different research group.

1. INTRODUCTION

Measurement techniques and experimental standards used by laser propulsion groups around the world often differ significantly even for commonplace measurements. Comparability is enhanced when similar measurements and standards are widely used. Thus, our intention for this paper is that it may spur the acceptance of common standards for measurements and data analysis to enable laser propulsion researchers to more rigorously test the validity of their own data as well as assess its importance in relation to previous studies.

The recent collaboration between the German Aerospace Center (DLR) and Nagoya University (NU) spurred a discussion which brought to light some key issues relating to standardization for laser propulsion. For example, how many measurements are necessary? What equipment, and what diagnostics, are necessary and sufficient? How can common measurement errors be avoided?

Upon reviewing the literature, we found that in general, difficulties in laser ablation propulsion measurements stemmed from misinterpretations or misunderstandings of five primary laboratory parameters; specifically, the laser pulse energy, laser pulse length, laser spot area, imparted impulse, and ablated mass. Therefore, in the interests of standardization, we will focus our discussion on these parameters. Some aspects have already been sketched in [1] and will be presented in more detail in this paper along with results from recent experiments.

2. METHODS AND PARAMETERS

In laser propulsion, the momentum coupling coefficient c_m plays a central role. Its most common unit, N/MW, indicates that it is a technical figure of merit giving the average thrust caused by a laser with a certain average power. In the case of pulsed laser propulsion, however, the defining fraction is usually augmented by time yielding the following definition:

$$c_m = \frac{\Delta p}{E_L} \tag{1}$$

where Δp is the imparted momentum of the target, e.g., caused by laser ablation at a given laser pulse energy E_L. Since lasers and methods of measuring the imparted momentum vary greatly, both aspects are studied in the following.

2.1. Cause: Parameters of the laser beam

2.1.1. Laser pulse energy

Not all energy detectors exhibit a uniform spatial response. This poses strong challenges for measurements made outside the strict limits set by the manufacturer. Beam output sizes vary widely, and the intensity of a beam focused onto the detector often exceeds the damage threshold. Especially in the case of a beam that is significantly smaller than the detector area the positioning of the beam on the detector is crucial. Hence, it is useful to determine the spatial response of the detector.

A scanning technique was used to check the spatial response of the detector. An aperture was fixed at a particular diameter, and also fixed relative to a probe laser beam at a stable portion of the laser beam, so that the total energy reaching the detector was constant. Diffraction does not significantly influence the energy measurement for this technique. The aperture size was sufficiently small to allow fine resolution of the detector surface that was scanned transverse to the beam in 2 dimensions.

An older detector (Gentec ED-500LIR) which had sustained minor damage to its measurement surface was tested at Nagoya University. For comparison, a calibrated pyrodetector (Ophir PE50BB) was scanned at DLR Stuttgart. The results are shown in Figure 1. Whereas the response of the damaged detector was non-uniform, the calibrated one exhibited a rather flat responsivity profile. However, the above data and an independent total energy measurement for absolute calibration allow for the accurate usage of the damaged detector as long as the illuminated area of the detector is specified.

Although laser profilometers may be used in beam characterization, these devices are often expensive, beyond the budget of most university research groups. However, standard measurements of the profile may still be made by scanning an aperture and detector across the beam. Proper implementation requires the detector and aperture to be transverse to the beam propagation axis and fixed relative to each other while scanned, so that the same detector area is illuminated at each scanned position. It is important that the same area on the detector is illuminated by the apertured portion of the laser beam at each scanning step, to avoid any position-dependent response on the active detector area. The aperture size should be sufficient to sample the beam energy, but small enough to avoid overlap (resulting in over-counting of energy).

The results of application of this technique are shown in Figure 2. With the DLR laser, an electron-beam sustained CO_2 high energy laser, a square aperture (1×1 cm^2) has been used with a step size of 1 cm. The NU laser, a TEA CO_2 laser (Selective Laser Coating Removal GmbH, model ML205E), was investigated with a circular aperture of 5 mm diameter and applying 5 mm step size. For each scan position, 3 shots (NU) and 5 shots (DLR), resp., have been taken yielding average

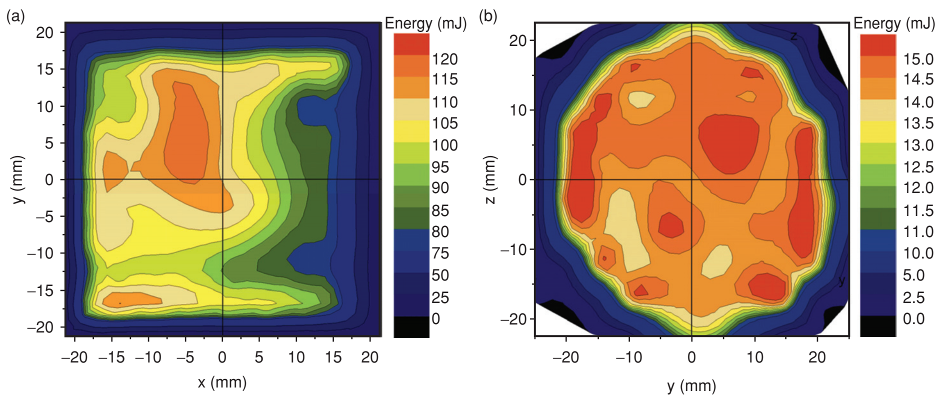

Figure 1. Responsivity of different pyrodetectors: Detected laser pulse energy with (a) damaged Gentec ED-500LIR detector (NU, aperture diameter: 5 mm, spatial resolution: 5 mm), (b) calibrated Ophir PE50BB detector (DLR, aperture: 3.5 mm, spatial resolution: 5 mm).

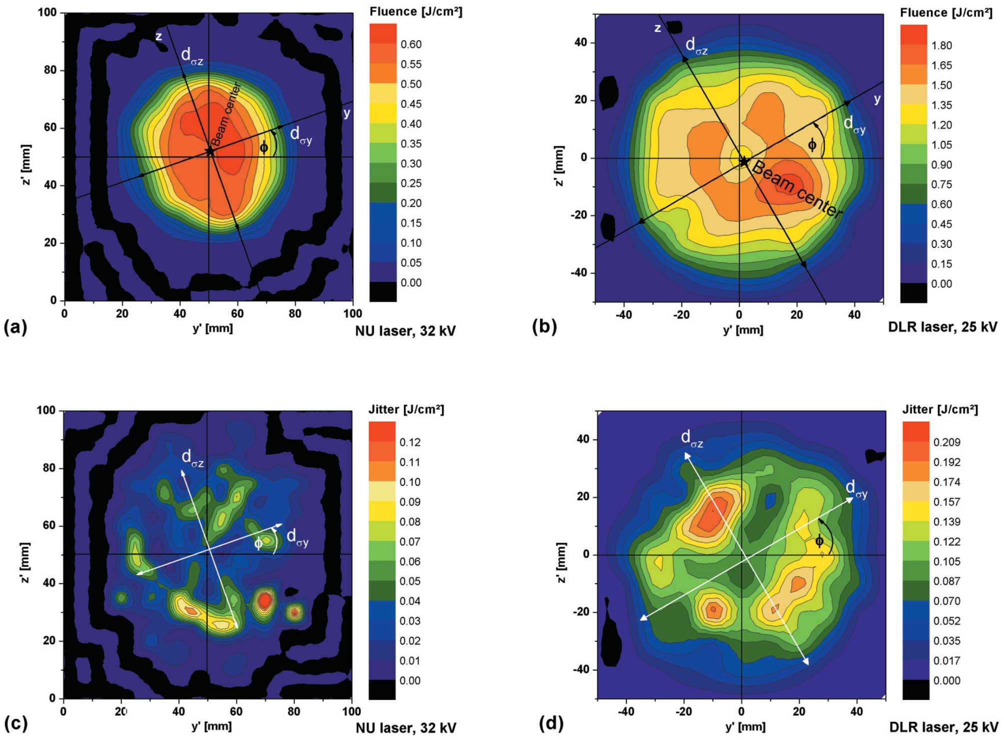

Figure 2. Beam profile and jitter of a SLCR TEA CO_2 laser (Nagoya University, (a), (c)) and an electron-beam sustained CO_2 high energy laser (DLR Stuttgart, (b), (d)). Corresponding beam parameters are depicted in Table 1. The principal axes of the beam profile are denoted with *y*, *z*, while *y′*, *z′* represent the axes of the laboratory system.

Table 1. Beam parameters derived from the analysis results shown in Figure 2.

Laser system	Beam center y'_0/z'_0 [mm]	Beam diameter $d_{\sigma y}/d_{\sigma z}$ [mm]	Orientation* φ [°]	Ellipticity ε [–]
NU	50.6/52.0	53.3/58.1	19.3	0.92
DLR	1.7/–1.3	84.9/83.2	30.1	0.98

*The orientation angle φ refers to the principal y-axis of the beam and y'-axis of the laboratory system.

fluence and pulse-to-pulse jitter. For energy measurement, ED-500-LIR (NU) and PE50BB (DLR), resp., pyrodetectors have been used.

This measurement technique not only allows for estimation of the total laser pulse energy, but also of the distribution of fluence across the laser beam. The shape of the beam is important for correct measurement and analysis of the laser spot area, as will be discussed in Section 2.1.3. Furthermore, characteristic beam parameters can be derived by means of first and second order moments of the fluence distribution, as described in detail in [2]. The corresponding results are shown in Table 1.

2.1.2. Laser pulse length

In laser ablation, the pulse length is often of understated importance; basic definitions of c_m ignore it, but its effect on impulse coupling is significant. As reported in [3], for the plasma regime,

$$c_m \propto \frac{1}{\sqrt[4]{I\lambda\sqrt{\tau}}} \tag{2}$$

whereas in the vapor regime, if a typical photothermal model is used, c_m increases with τ,

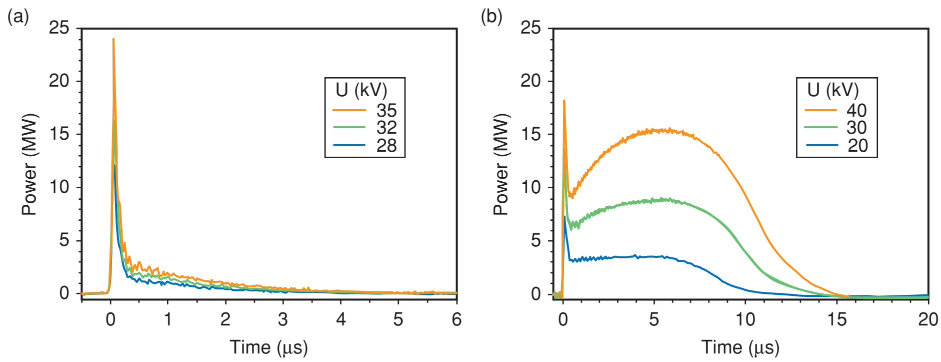

Figure 3. Temporal pulse shape of the CO_2 lasers at Nagoya university (a) and DLR (b) at various main discharge voltages.

$$c_m \propto \sqrt[4]{\tau} \tag{3}$$

if the minor dependence of the ablation threshold:

$$\Phi_a \propto \sqrt{\tau} \tag{4}$$

which appears under a logarithm in the denominator, is neglected. From first principles, the photochemical model for low fluence (i.e., below the plasma threshold) does not appear to possess an inherent dependence on the pulse length.

From the temporal courses of the laser pulse at DLR and NU, cf. Figure 3, it can be seen that the overall pulse length differs by nearly one magnitude, since the high energy laser beam exhibits a pronounced tail that enlarges and prolongs with increasing main discharge voltage which is proportional to the pulse energy (31 ± 2 to 149 ± 14 J). For the moderate pulse energies of the laser at NU (5 to 10 J), the tail is less pronounced and shows an exponential decay. Different pulse lengths, however, should lead to deviating results concerning the measurement of the impulse coupling coefficient. From Relations 2 and 3 it can be derived that the given deviation of one magnitude between these two lasers yields a diminished c_m by a factor of 0.75 for the longer pulse in the plasma regime, while at lower fluences for the longer pulse c_m is enhanced by a factor of 1.78. This issue should be carefully considered when comparing results from different scientific groups.

2.1.3. Laser spot area

The accurate determination of the laser spot area is critical for fluence measurement, since fluence is defined as laser pulse energy divided by spot area. Fluence should depend significantly on the distance from the laser source and any mirrors or lenses that interact with the beam, based on attenuation, divergence and diffraction, which influence the transverse spatial distribution of the energy. The standard definition for the laser spot area is the diameter of a circular aperture at which ~ 86.5% of the total pulse energy (or power) is measured on a detector behind that aperture, when centered on the beam [5]. At this diameter, $1/e^2$ of the incident energy (or power) is stopped by the aperture. Alternatively, the ablated spot size may be considered. In that case, the definition of the spot size may need to be adapted with account for the specific target material to represent the area within which the incident fluence exceeds the ablation threshold. For instance, ablated spot area can be measured directly from visible ablation patterns on a target surface [6]. In the common case of elliptical spot areas, measurements should at least be made along the major and minor diameters of the ellipse. Thermal paper was often used in laser propulsion studies [7, 8, 9] and sometimes polymers (*e.g.*, fiber-filled polyvinylchloride [10, 11]) have also been used which show high-contrast ablation patterns. The widespread use of thermal paper in laser propulsion studies is probably due to its low cost, availability (e.g., as fax and receipt papers), and convenience. In fact, the outer diameter of an ablation pattern is insufficient to define an ablated spot size, regardless of the material. Such diameters usually change significantly with changes in total laser pulse energy, if other parameters are held constant. Most importantly, the threshold fluence must be known if the approach in [6] is to be correctly followed, and shots at different beam energies are

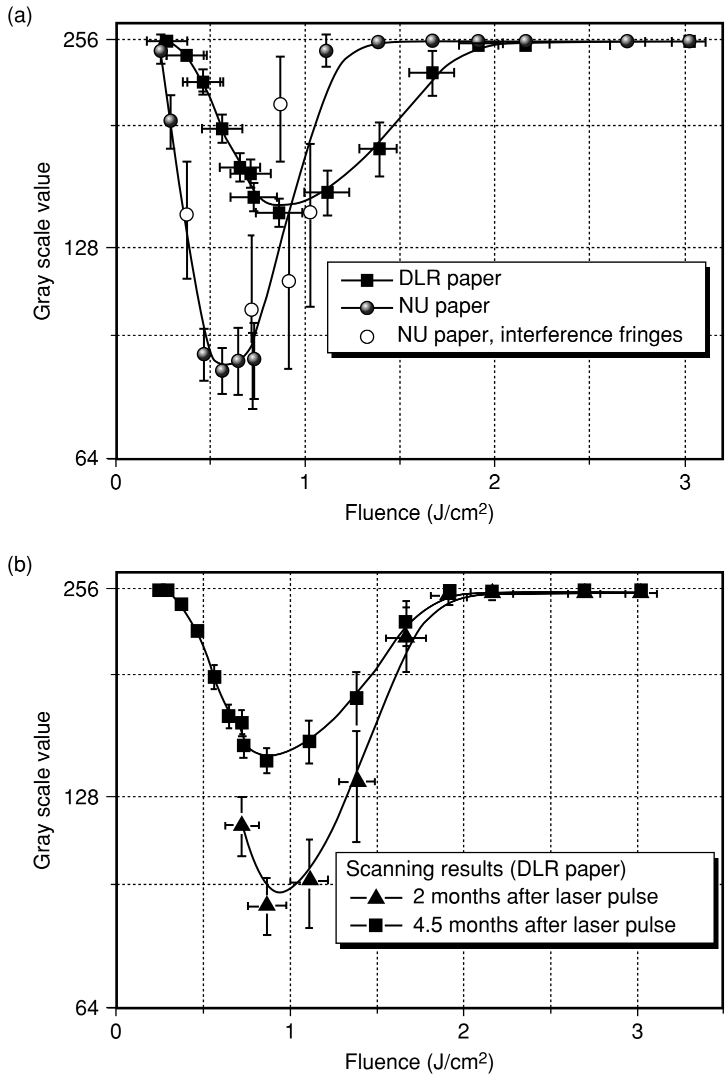

Figure 4. Sensitivity of different thermal papers (a) and aging effects (b). On an 8-bit greyvalue scale, "255" corresponds to white and "0" to black.

necessary to construct a meaningful understanding of the spot area contours. A specific kind of thermal paper has an associated threshold energy to produce a visible effect on the paper surface; this threshold can vary significantly between manufacturers and across paper types.

During a collaborative research exchange, thermal papers used at DLR and NU were compared. A central spot (8 mm diameter) of the large (around 80 mm diameter), nearly top hat laser beam at DLR was analyzed with respect to (apertured) pulse energy and coloring of a thermal paper at that position. The results are shown in Figure 4. With the NU paper, some data had to be disregarded because of interference fringes from the aperture leading to an inhomogeneous coloring.

The intensity of coloring of the burn pattern strongly depends on the incident fluence, as shown in Figure 4. A significant coloring is noted for the DLR paper around 0.88 J/cm^2 in the range of 0.53 J/cm^2 to 1.53 J/cm^2 (FHWM). The onset of bleaching with higher fluences can be ascribed to ablation (combustion and even plasma ignition) from the paper surface which was detected by photographs and high speed recordings. However, the NU paper shows a greater sensitivity than the DLR paper. The strongest coloring appears at 0.57 J/cm^2, and it can be applied for a range of 0.32 J/cm^2 to 0.98 J/cm^2 (FHWM). Hence, spot area measurements vary with the type of thermal paper employed.

Figure 5 shows thermal burn patterns on DLR paper of the entire beam of the DLR high energy laser. With high pulse energies (a), the incident fluence causes nearly uniform ablation throughout the spot while the steep edge of the spatial profile leaves a thin torus, cf. the beam profile in Figure 2(b). In

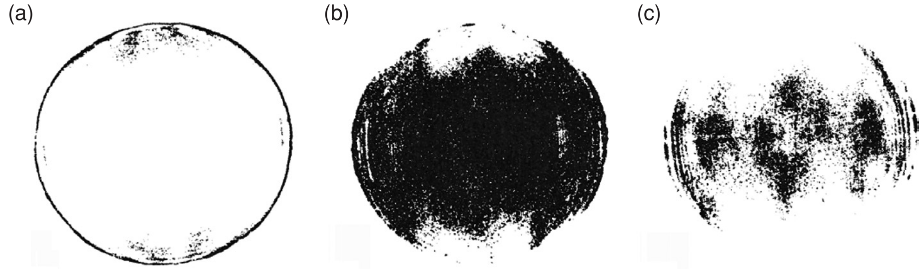

Figure 5. Marks on thermal paper from a laser pulse of the DLR high energy laser at 103 ± 6 J (a), 46 ± 3 J (b), and 32 ± 2 J (c).

experimental work, this is a good approximation for the beam diameter. At lower pulse energies, cf. Figure 5(b) + (c), it is rather difficult to determine the beam diameter on one or even on both axes, since the threshold fluence for coloring is only partly exceeded inside the spot area. Nevertheless, assuming that the normalized fluence distribution is independent from the pulse energy, a series like Figure 5(a) – (c) can be regarded as a tomography of the fluence distribution with different thermal papers exhibiting an equivalent central sensitivity of 0.28 J/cm^2 (a), 0.63 J/cm^2 (b), and 0.9 J/cm^2 (c). This approach allows for a fine resolution of the fluence distribution, e.g. revealing a fringe structure inside the spot (c).

2.2. Effect: Propulsion parameters

2.2.1. Imparted impulse

Several methods can be used to measure the impulse imparted on a laser-driven target. AFRL and DLR previously studied the use of impulse pendula for ablation measurements [9]. Other studies have considered torsion pendula [8, 12, 13]. The use of piezoelectric force sensors for ablation measurements was spearheaded by UAH, although some measurement challenges remain, e.g., addressing frequency cutoffs, impulse reflection [14], restitution behavior of targets [15], and minimization of noise from metal-to-metal impacts.

Since laser propulsion is an aerospace issue, launches were investigated by many groups [22, 16, 17, 18]. In launch experiments with a parabolic thruster, coupling coefficients were often found to be slightly higher than results from an impulse pendulum [25]. This effect may be explained by the reduction of degrees of freedom in a pendulum. Hence, both perfect alignment of the target with the laser beam and matching of the thrust vector direction with the pendulum measurement direction are required. If the latter condition is not met, only the projection of the thrust vector on the pendulum's measurement axis will be displayed and c_m will be underestimated. If misalignment against the laser beam occurs, some of the energy will be imparted into lateral and rotational components. However, suppression of the corresponding degrees of freedom in a pendulum setup might obscure the necessity of re-alignment and can indirectly lead to an underestimation of c_m which would be higher in the case of perfect alignment to the laser beam, as e.g. shown for a parabolic thruster in [22]. In practice, great care should be taken on the alignment of the whole experimental setup. 3D tracking of a free flight can be applied to reconstruct the entire impulse vector, but even in this case, losses can still occur due to damped vibrations of the vehicle body. A sample experiment is described in Section 3.

2.2.2. Ablated mass measurement

It is typical to use a laboratory balance for measurements of ablated mass. Different balances have disparate sensitivity and measurement limits. It is important to note that the 'readability' of a device is merely the smallest change possible to be registered by the instrument. Such a change may not be meaningful, and is usually not equivalent to the accuracy of the instrument; in fact, the accuracy is typically at least a factor of 2-3 times the readability. Typical accuracy limits for balances range from 10 to 1000 μg. Unfortunately, large load mass range tends to pair with low sensitivity, and vice versa, which restricts target sizes for experiments. The cost of a balance scales with both measurement accuracy and load mass range.

One attractive capability would be the on-site measurement of mass under vacuum. Generation of ambient pressures interesting for laser propulsion research; e.g., 10^{-3} Pa, similar to low earth orbit, usually requires significant pump down times. Consequently, repetitively venting a large vacuum chamber after each shot (or series of shots) to allow mass measurements represents a significant time cost, and can be a major obstacle to an efficient measurement campaign. Some modern balance manufacturers now offer vacuum balances with real-time measurement capabilities, but they are prohibitively expensive, often ~$10,000 US. Alternatives such as custom-adaptation of an expensive, in-air scientific balance for use in a vacuum chamber should only be undertaken with caution, and should be accompanied by careful calibration. However, a balance's performance might as well be unaffected from the operation in vacuum.

New techniques are still needed to measure small changes in mass on large ablation targets in real time. One example of a technique for ablated mass measurement is surface profilometry. In this technique, the target surface is scanned to reconstruct a spatially resolved depth. The volume and ablated mass associated with an ablation crater may thereby be estimated; however, changes in density (e.g., bubble formation in volume, common in ablation of polymers such as polymethylmethacrylate) could cause misinterpretation of such data. Profilometry can also provide feedback for beam diagnostics (e.g., for laser spot area measurement and diffraction effects). Modern profilometry techniques are usually applied in atmospheric air conditions; however, a properly-designed profiling instrument could accurately scan target surfaces in vacuum, possibly even on the timescale of the ablation event.

3. SAMPLE EXPERIMENT

The measurement of the impulse coupling coefficient is illustrated and discussed at a simple free flight experiment of a laser-driven device. It is referred to as "lightcraft", a term that Myrabo introduced for "[…] any flight platform, airborne vehicle, or spacecraft designed for propulsion by a beam of light – be it microwave or laser […]" (cited from [19]).

3.1. Experimental setup

In this experiment, the lightcraft consists of a parabolic mirror, a propellant rod and a protective cap. The parabolic mirror, cf. Figure 6(a), is made from aluminum with a wall thickness 0.5 mm. Its focal length is 10 mm and it focuses the incoming laser pulse to the side of the propellant rod (circular focus). Furthermore, its bell-shaped geometry acts as a nozzle for the expanding gas.

The propellant rods are made of Delrin™ (polyoxymethylene, POM). POM exhibits a strong absorption peak around 10.6 μm [20] and is well-suited for laser propulsion experiments since a relatively high thrust is generated with only little contamination of the optics by soot from combustion. Three different rod diameters (8, 10, 12 mm) were tested for comparison.

In order to protect the lightcraft from damage, a lightweight cap of polyamide fabricated by laser sintering was mounted on top of the reflector. Additionally, a huge net was spanned around the launchpad to catch the lightcraft.

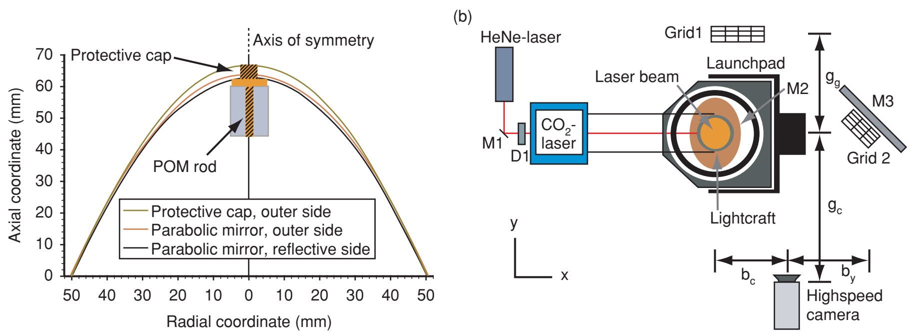

Figure 6. Scheme of the parabolic thruster (a) with propellant rod and protective cap. For laser propulsion experiments, the thruster was placed on a launchpad consisting of 3 steel rods in a 120° configuration above the high energy laser beam directed towards the ceiling by mirror M2. The experimental setup is shown in (b). Flights were recorded with a high speed camera from the side. Reference grids provided for calibration of flight data in the x-z plane (grid #1) and y-z plane (grid #2).

The lightcraft was powered by a pulsed, electron-beam sustained CO_2 high energy laser. It is refered to in Section 2 as "DLR laser" and described in greater detail in [21]. For alignment purposes, a HeNe laser is guided through a small aperture (5 mm diameter) in the center of the rear reflector of the resonator cavity. At the time of the CO_2 laser pulse, the HeNe was blocked by a pyrodetector (D1), PE 50-BB by Ophir Electronics Ltd. connected to a Laserstar Dual Channel control unit. In this experiment, it registered a small fraction (0.159 ± 0.006 %) of the outcoupled laser pulse energy at the rear side.

A large mirror (M3) provides for a stereo view of the flight path allowing for a full 3D analysis. The flights were recorded with a highspeed camera, MotionScope M3 by Redlake, set at a temporal resolution of 500 fps.

3.2. Data analysis

Small markers were painted on the protective cap of the lightcraft for tracking purposes. Video data tracking was carried out with a Motion Studio Software, Version 2.07.08, by IDT Vision. The image data were calibrated by means of grid 1 and 2, resp., taking into account spatial distortion (g_g = 0.24 m, g_c = 2.98 m, b_c = 0.15 m, b_y = 0.46 m). The tracking data were thoroughly examined for outliers due to artifacts in semi-automatic tracking. For each video frame, the position of the lightcraft's center of mass (CMS) was reconstructed from the positions of the markers on the lightcraft. The theoretical foundation of this calculation is described in detail in [22].

The temporal courses of altitude and lateral offset were fitted polynomially and linearly, resp., in order to derive the velocity increment at the time of the laser pulse. All three velocity components were added vectorially.

The lightcraft was weighed after each laser pulse on a laboratory balance with 1 mg readability. The impulse coupling coeffient was deduced from data on velocity increment, lightcraft mass and laser pulse energy.

The spot area on the propellant rods was modeled with Optica 3.0 from Wolfram Research approximating the laser beam by a grid of rays with 1 mm pitch comprising 5025 rays taking into account divergence based on beam quality measurements [23].

3.3. Results and discussion

Lateral impulse components amounted to only around (3.1 ± 1.0) % of the impulse in the z-direction. Hence, vectorial addition of all impulse components yielded an overall impulse only slightly higher than the impulse measured in the z-direction. In this experiment, a measurement of the CMS movement only in the z-direction would lead to an underestimation of the total impulse by only (0.05 ± 0.04) %.

The data derived from the measurements are shown in Figure 7. The results obtained for 10 mm and 12 mm rod diameter are similar within the range of the corresponding error bars. For laser pulse energies larger than 50 J the imparted momentum is clearly greater than in the case of 8 mm rod diameter. This can be attributed to the lower mass removal, since the spot area is significantly smaller. In this range, c_m also decreases with the fluence. However, additional removal does not lead to a visibly enhanced impulse, since the data for 10 mm and 12 mm are very similar. Hence, there seems to be an optimum configuration for a cylindrical propellant inside this parabolic nozzle at 10 mm rod diameter with respect to maximum impulse coupling and minimum propellant consumption. Therefore it is desirable to develop a model for the impulse coupling characteristics of this specific laser ablative propulsion configuration.

Analyzing the various components of the resulting impulse, two references from different experimental setups have been inserted in Figure 7. Reference #1 describes the imparted momentum on the parabolic thruster in the case of a laser-supported detonation from air breakdown inside the chamber at various laser pulse energies [22]. In a simplistic approach, we assume for the coupling coefficients

$$c_m^{(n,a)} = c_m^{(n)} + c_m^{(a)} \tag{5}$$

where $c_m^{(n,a)}$ refers to ablation inside a nozzle, $c_m^{(n)}$ refers to air breakdown inside a nozzle and $c_m^{(a)}$ refers to ablation from an unconfined, flat target. Model data for the latter experimental setup from [20] have been adapted to the corresponding ablation areas in the experiment inside the nozzle for comparison and are shown as reference #2 in Figure 7. However, it can be clearly seen in most of the

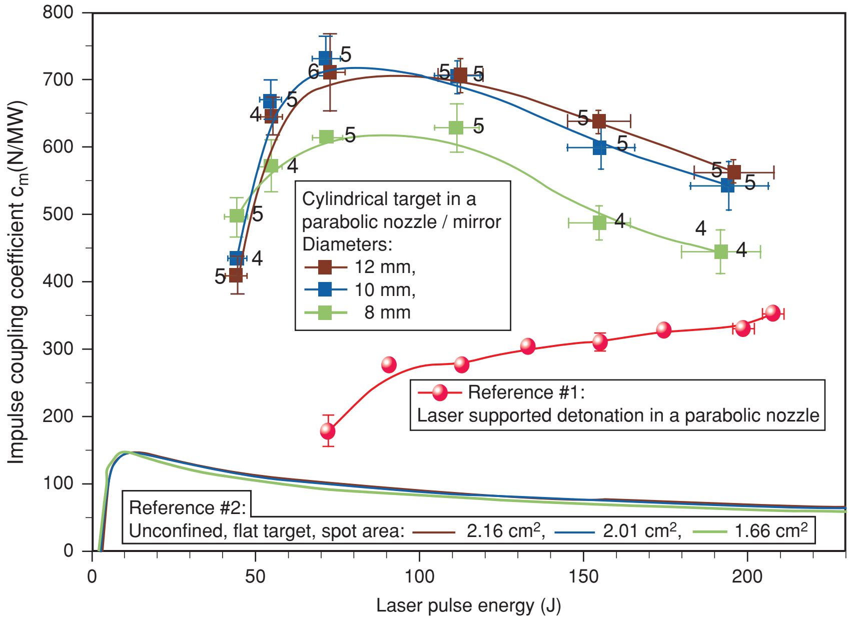

Figure 7. Impulse coupling resulting from ablation on a cylindrical rod inside a parabolic thruster is depicted for various pulse energies and rod diameters. The number of data points is given close to the corresponding symbol. Experimental data from a laser-supported detonation without propellant [22] and model data for laser ablation from a flat, unconfined POM target with a similar ablation area [20] are given for comparison.

cases that the imparted impulse with propellant inside a nozzle exceeds even the sum of these two reference components.

Hence, the question of comparability arises with respect to standardization of the measurement of c_m. The data of reference [22] have been derived under the same conditions as the sample experiment. In [20], the laser pulse length was one order of magnitude lower. However, this would even lead to a decrease of c_m at the sample experiment according to Relation 2. A major difference between both experiments is the difference between the ablation spots: While ablation spots from a laser with a top hat beam profile leave a rather flat and uniform ablation crater on the propellant surface, ablation traces on a cylindrical rod on the axis of the parabolic reflector exhibit a thin and deep peak and a broad and shallow tail. These findings were verified by raytracing analysis of the corresponding intensity distribution. The spot area was defined with respect to the ablation threshold of POM at $\lambda = 10.6$ µm, $\Phi_{tr} = 1.35 \pm 0.06$ J/cm^2 [20]. However, the comparability of these different spot types is doubtful and leaves some uncertainty since the model data from [20] depend on the fluence. Finally it should be noted that the database for that model was built using a force sensor which might imply systematic deviations from free flight experiments.

Nevertheless, ablation from a flat target may not be appropriate to represent the specific ablative component of c_m in the sample experiment. When laser-induced plasma is generated, an absorption wave is generated that travels towards the laser source shielding the target from the laser. In the case of a flat target, this effect lowers the imparted momentum [24]. The impulse may be increased, however, in the case of a target that is illuminated on a focal ring inside a parabolic mirror. Then, the expanding plasma is heated before it reaches the reflector walls. Hence, the laser pulse energy deposited in the absorption wave can be used - at least partly - for thrust generation. Therefore, we can rewrite Equation 5 as

$$c_m^{(n,a)} = c_m^{(n)} + \gamma^{(0)} c_m^{(a)} \tag{6}$$

where $\gamma^{(0)}$ denotes the impulse gain with respect to a flat target based on optical effects like the absorption wave inside a reflector acting as a nozzle. A rough estimation of the impulse gain is given in Table 2.

Table 2. Impulse gain $\gamma^{(o)}$ derived from the comparison of data depicted in Figure 7.

Propellant diameter [mm]					
8		10		12	
E [J]	$\gamma^{(o)}$ [–]	E [J]	$\gamma^{(o)}$ [–]	E [J]	$\gamma^{(o)}$[–]
72 ± 5	4.6 ± 0.6	71 ± 4	5.5 ± 0.8	73 ± 4	5.2 ± 0.8
111 ± 7	4.3 ± 0.3	111 ± 7	4.9 ± 0.2	112 ± 7	4.8 ± 0.2
155 ± 9	2.5 ± 0.2	155 ± 10	3.8 ± 0.3	154 ± 10	4.1 ± 0.2
192 ± 12	1.7 ± 0.1	194 ± 12	3.0 ± 0.2	196 ± 12	3.2 ± 0.1

4. CONCLUSIONS

Although a wide range of measurement techniques is used to study laser propulsion, it is the hope of the authors that some significant agreement may be reached about standards for such measurements to produce comparable experiments and increase the quality of research. Such standards should be based on direct measurement parameters of maximal importance, including the laser pulse energy, pulse length, spot area, ablated mass, and imparted impulse. We already experienced great benefit from international cooperation on this issue exploring new topics for future research, e.g. in the field of supplementary thrust generation by interaction of an absorption wave with a reflective thrust chamber.

ACKNOWLEDGEMENTS

Financial support by DLR funds for International Cooperation is gratefully acknowledged. Additional support was provided through a 2009 Global Center of Excellence Young Researcher Award (Dr. John Sinko). Support was also provided by Nagoya University and the Micro-Nano Division of the Global Center of Excellence.

The authors want to thank Sebastian Walther for technical assistance in the laboratory and Eric Wollenhaupt for video data tracking.

REFERENCES

[1] Sinko, J.E., Scharring, S., Eckel, H.-A., Röser, H.-P., and Sasoh, A., Measurement Issues In Pulsed Laser Propulsion, in: Phipps, C.R., Komurasaki, K., and Sinko, J.E., eds, *Proceedings of the Sixth International Symposium on Beamed Energy Propulsion, AIP Conference Proceedings,* American Institute of Physics, Melville, New York, 2010, 1230, 125–136.

[2] Lasers and laser-related equipment – Test methods for laser beam widths, divergence angles and beam propagation ratios – Part 1: Stigmatic and simple astigmatic beams, *ISO 11146-1:2005(E),* ISO copyright office, Geneva, 2005.

[3] Phipps, C., Turner, T., Harrison, R., York, G., Osborne, W., Anderson, G. Corlis, X., Haynes, L. Steel, H. Spicochi, K, and King, T., Impulse Coupling to Targets in Vacuum by KrF, HF and CO_2-Lasers, *Journal of Applied Physics,* 1988, 64, 1083–1096.

[4] Phipps, C., Birkan, M., Bohn, W., Eckel, H.-A., Horisawa, H., Lippert, Th., Michaelis, M., Rezunkov, Yu., Sasoh, A., Schall, W., Scharring, S., Sinko, J., Reciew: Laser-Ablation Propulsion, *Journal of Propulsion and Power*, 2010, 26(4), 609–637.

[5] Lasers and laser-related equipment – Test methods for laser beam widths, divergence angles and beam propagation ratios – Part 3: Intrinsic and geometrical laser beam classification, propagation and details of testmethods, ISO11146-3:2004(E), ISO copyright office, Geneva, 2004.

[6] Decker, J.E., Xiong, W., Yergeau, F., and Chin, S. L., Spot-size measurement of an intense CO_2 laser beam, *Applied Optics*, 1992, 31(12), 1912–1913.

[7] Watanabe, K. and Sasoh, A., Laser impulse generation required for space debris deorbiting, in: *Proceedings on High-Power Laser Ablation V, Proceedings of SPIE*, 2004, 5448, 422–427.

[8] Suzuki, K, Sawada, K., Takaya, R., and Sasoh, A., *Journal of Propulsion and Power,* 2008, 24(4), 834–841.

[9] Schall, W. O., Bohn, W. L., Eckel, H.-A., Mayerhofer, W., Riede, W., Walther, S., and Zeyfang, E., US German Lightcraft Impulse Measurements, Final Report, SPC00-4033, EOARD contract F61775-00-WE033, Apr. 2001.

[10] Sinko, J.E. and Gregory, D.A., Vaporization - Driven Impulse Generation for Laser Propulsion, in: *43rd AIAA/ASME/SAE/ASEE Joint Propulsion Conference & Exhibit, AIAA Paper 2007–5601.*

[11] Phipps, C., Luke, J., Lippert, T., Hauer, M., and Wokaun, A., Micropropulsion Using a Laser Ablation Jet, *Journal of Propulsion and Power,* 2004, 20(6), 1000–1011.

[12] Phipps, C.R., Luke, J.R., Helgeson, W., and Johnson, R., A ns-Pulse Laser Microthruster, in: Komurasaki, K., Yabe, T., Uchida, S., and Sasoh A., eds., *Fourth International Symposium on Beamed Energy Propulsion, AIP Conference Proceedings,* American Institute of Physics, Melville, New York, 2006, 830, 235–246.

[13] D'Souza B.C. and Ketsdever, A.D., Direct Impulse Measurements of Ablation Processes from Laser-Surface Interactions, in: *36th AIAA Plasmadynamics and Lasers Conference, AIAA Paper* 2005-5172.

[14] Sterling, E., Lin, J., Sinko, J., Kodgis, L., Porter, S., Pakhomov, A.V., Larson, C.W., and Mead, F.B.Jr., Laser-Driven Mini-Thrusters, in: Komurasaki, K., Yabe, T., Uchida, S., and Sasoh A., eds., *Fourth International Symposium on Beamed Energy Propulsion, AIP Conference Proceedings,* American Institute of Physics, Melville, New York, 2006, 830, 247–258.

[15] Sinko, J.E. and Lassiter, J.S., Sphere-Wall Impact Experiments with Piezoelectric Force Sensors, in: Pakhomov, A. V., ed., *Fifth International Symposium on Beamed Energy Propulsion, AIP Conference Proceedings*, American Institute of Physics, Melville, New York, 2008, 997, 131–142.

[16] Michaelis, M.M., Moorgawa, A., Forbes, A., Klopper, W., McKenzie, E., Boutchiama, D., and Bencherif, H., Laser Propulsion Experiments in South Africa, in: Phipps, C.R., ed., *High-Power Laser Ablation IV, Proceedings of SPIE,* 2002, 4760, 691–695.

[17] Watanabe, K., Takahashi, T., and Sasoh, A., Useful In-space Impulse Generation Powered by Laser Energy, in: Komurasaki, K., ed., *Second International Symposium on Beamed Energy Propulsion, AIP Conference Proceedings*, American Institute of Physics, Melville, New York, 2004, 702, 115–121.

[18] Myrabo, L.N., Brief History of the Lightcraft Technology Demonstrator (LTD) Project, in: Pakhomov, A.V., ed., *First International Symposium on Beamed Energy Propulsion, AIP Conference Proceedings,* American Institute of Physics, Melville, New York, 2003, 664, 49–60.

[19] Myrabo, L.N. and Ing, D., *The Future of Flight,* Baen Books, Simon & Schuster, 1985.

[20] Sinko, J., *Vaporization and shock wave dynamics for impulse generation in laser propulsion,* PhD thesis, University of Huntsville, Alabama, 2008.

[21] Mayerhofer, W., Zeyfang, E., and Riede, W. Design data of a repetitively pulsed 50 kW Multigas Laser and recent experimental results, *XII International Symposium on Gas Flow and Chemical Lasers and High-Power Laser Conference, Proceedings of SPIE,* 1998, 3574, 644–648.

[22] Scharring, S., Hoffmann, D., Eckel, H.-A., and Röser, H.-P., Stabilization and steering of a parabolic laser thermal thruster with an ignition device, *Acta Astronautica,* 2009, 65, 1599–1615.

[23] Scharring, S., Hoffmann, D., Eckel, H.-A., and Röser, H.-P., Remotely Controlled Steering Gear For A Laser-Driven Rocket With A Parabolic Thruster, in: Phipps, C.R., Komurasaki, K, and Sinko, J.E., eds, *Proceedings of the Sixth International Symposium on Beamed Energy Propulsion, AIP Conference Proceedings,* American Institute of Physics, Melville, New York, 2010, 1230, 89–100.

[24] Eckel, H.A., Tegel, J., and Schall, W.O., CO_2 laser absorption in ablation plasmas, in: Komurasaki, K., Yabe, T., Uchida, S., and Sasoh A., eds., *Fourth International Symposium on Beamed Energy Propulsion, AIP Conference Proceedings,* American Institute of Physics, Melville, New York, 2006, 830, 272–283.

[25] Scharring, S., Eckel, H.-A., and Röser, H.-P., Flight Analysis of a Parabolic Lightcraft - Ground-based Launch, in: Pakhomov, A.V., ed., *Fifth International Symposium on Beamed Energy Propulsion, AIP Conference Proceedings*, American Institute of Physics, Melville, New York, 2008, 997, 304–315.